Toughening effect of non-periodic fiber distribution on crack propagation energy of UHTC composites

Toughening effect of non-periodic fiber distribution on crack propagation energy of UHTC composites

S. Failla[a,b], P. Galizia[a,]*, L. Zoli[a], A. Vinci[a], D. Sciti[a]

[a] CNR-ISTEC, National Research Council of Italy - Institute of Science and Technology for Ceramics, Via Granarolo 64, I-48018 Faenza, Italy

[b] University of Parma, Department of Chemistry, Life Science and Environmental Sustainability, Parco Area della Scienza 11/a, 43124 Parma, Italy

*corresponding author, email: pietro.galizia@istec.cnr.it

Abstract

Different configurations of continuous carbon fiber-reinforced ultrahigh temperature ceramics (UHTCs), by combining coatings and matrix, were produced via electrophoretic deposition (EPD) and slurry infiltration. The toughening of non-periodic fiber distribution induced by the EPD process was investigated through work of fracture analysis. The results show that a non-periodic fiber distribution results in toughness increase from 8 MPa√m to 11 MPa√m with respect to a periodic fiber distribution. This toughness improvement does not strongly affect the flexural strength, which is mainly related to the fiber volumetric amount. It is shown that the assembling of carbon fibers into bundles (i.e. by dispersing the fibers with a non-periodic distribution) increases the crack propagation energy dissipated on the crack-wake from 0.5 kJ/m^2 to 1 kJ/m^2, which can be mainly ascribed to the fiber pull-out. On the other hand, the energy dissipated on the crack-tip (as fiber/matrix debonding) is fiber distribution-independent

and increases from 0.3 kJ/m^2 to 0.4 kJ/m^2 with increasing the fiber amount from 33 vol% to 40 vol%. Finally, WoF analysis is proposed as test to evaluate pull-out toughening instead of push-in and push-out tests.

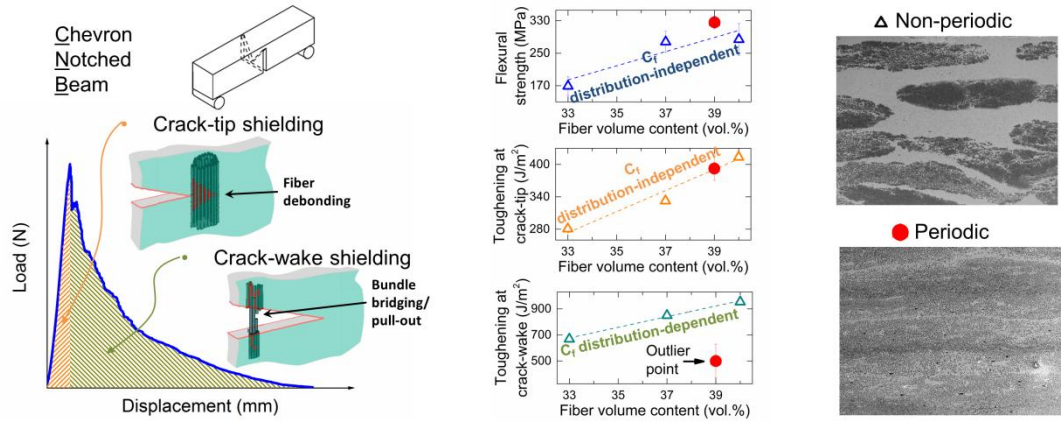

Keywords: ceramics; coating materials; composite materials; mechanical properties; electrophoretic deposition (EPD).

1. Introduction

Ultra-high temperature ceramics (UHTCs) are a class of ceramic refractory materials very interesting for their high melting point (>3200 °C), chemical stability, and resistance to erosion and ablation. For these reasons, carbides and borides, such as ZrB_2, TiB_2, HfB_2, HfC, TaC [1-4], are potential candidates to make components which work in extreme thermal and chemicals environment condition; hypersonic flight, thermal protection system (TPS), sharp leading-edge in re-entry vehicles in atmosphere and nozzles for rockets [5,6]. ZrB_2 and TiB_2 have low theoretical density and high thermal conductivity, but suffer from poor fracture toughness and thermal shock resistance [1]. Ceramic Matrix Composites (CMCs), C/C and C/SiC, represent the class of materials

currently used in aerospace filed as TPSs and propulsion components [7,8]. They are attractive because, by comparison with UHTCs, have excellent mechanical properties and low specific weight, but suffer from poor oxidation resistance above 1600°C even if they contain borides as secondary phase [11].

The idea of combining these two classes of materials (UHTCMCs) was thought to take the best properties of both materials: wisely combining qualities of CMCs and UHTCs we get improved erosion/ablation resistance compared to pure CMCs, improved damage tolerance and thermal shock compared to UHTCs and intermediate specific weight [9-12].

Electrophoretic deposition (EPD) is a simple and efficient colloidal process which can be used in several areas [13]. Electric field is established between two electrodes immersed in a stable colloidal suspension wherein ceramics bodies (working electrode) are shaped directly. In this condition the charged particles, dispersed in a solvent, move toward the working electrode under applied DC electric field [14,15]. This is a good method to create a thick coating of different materials onto conductive substrates [16]. So far many studies have been carried out on EPD coating of fiber in order to produce metal matrix composites (MMCs) [17], CMCs [18], or just to use the fiber as a template for replicas of different kinds of ceramics [19]. In case of continuous fiber-reinforced composites, the coating mainly aims to (i) control interface debonding and frictional sliding in order to increase the crack-wake bridging phenomena and subsequent toughness [18,20,21], and (ii) protect from degradation at high temperature [22]. Recently, EPD technique has been exploited to assemble the carbon fibers into bundles, the so called “salami-inspired” architecture that produces an alternating of strong and

weak interfaces [23]. This trick allows to achieve the best compromise between the matrix-to-fiber stress transfer, and crack deflection and pull-out [23].

Dispersion and co-dispersion of ZrB_2 and/or SiC have been reported in the literature [24-27], as well as EPD of ZrB_2-SiC films starting from aqueous suspensions [26,28]. The main problem of water based suspension is the electrolysis of water which can result in large and irregularly distributed flaws [26,28]. Furthermore electrochemical reactions can occur on the surface of the metal electrode when current are passing off. For these reasons, many researchers prefer the use of organic solvent, even if they are not eco-friendly [29-32].

In this study, we exploit EPD to produce salami-inspired architectures (called non-periodic structures in the following) ZrB_2 and TiB_2 coatings on carbon fabrics. The mechanical properties of the final components are investigated and compared to a similar UHTCMC in terms of fiber volume content and porosity, but characterized by uniformly distributed carbon fibers (below called periodic structure). In particular, fracture energy analysis, based on load-displacement curves obtained from four point bending tests of chevron notched beams, is used to determine if mechanical properties are just affected by the fiber volume content (FVC), or by both FVC and fiber distribution degree. By integrating the area below the load/displacement curve it is possible to obtain the values of work of fracture (WoF) pre- and post-peak, W_T and W_W respectively, which can be correlated to the toughening mechanism acting on the crack tip and on the wake of the crack.

2. Experimental part

2.1. Materials

Commercial powders were used for the materials' production: ZrB_2 (H.C. Starck, Germany, impurity max content: C: 0.25 wt%, O: 2 wt%, N: 0.25 wt%, Fe: 0.1 wt%, Hf: 0.2 wt%, particle size range 0.1-8 µm). TiB_2 (H.C. Starck, Grade F, Germany, impurity max content: O: 2 wt%, particle size range 2.5-3.5 µm), and B_4C (H.C. Starck, Grade HS, Germany, B:C ratio 3.7-3.8 particle size range 0.8 µm). Carbon fibers (Granoc XN80-6K: density 2.17 g/cm^3, fabric thickness 330 µm, mass per unit area 330 g/m^2, fiber diameter 10 µm, sized with epoxy resin about 1 wt%, CTE -1.5 10^{-6}/K, tensile modulus of 780 GPa and tensile strength 3.4 GPa) were used as substrate in EPD. Ethanol-based colloidal suspensions at 2 wt% of either ZrB_2 or TiB_2 for EPD process were prepared by ball-milling for 3 h in a polyethylene bottle with SiC balls. Depositions on individual unidirectional (UD) C_f fabrics are performed in plane-parallel cell geometry and cathodic modality, keeping the working electrode 10 mm apart from the stainless steel counter electrode and applying constant DC potentials (Digimaster PS3003DB). After EPD process, the coated fabrics were infiltrated with slurries having compositions ZrB_2 + 5 vol% B_4C or TiB_2 + 5 5 vol% B_4C, subsequently stacked in 0/0° configuration and dried using the vacuum bagging technique at 90°C. B_4C was added as sintering aid, according to previous studies [33]. The schematic flow diagram of the green shaping is illustrated in Fig.1. Three different combinations of coating and matrix were produced, see Table1. Finally, sintering was carried out by hot pressing in low vacuum range using an induction-heated graphite die with a uniaxial pressure of 30-40 MPa, at 1800-1900°C. For the sake of comparison, an uncoated sample was also

produced with the same composition of ZrB_2+5 vol% B_4C, just using the slurry impregnation and sintering [9].

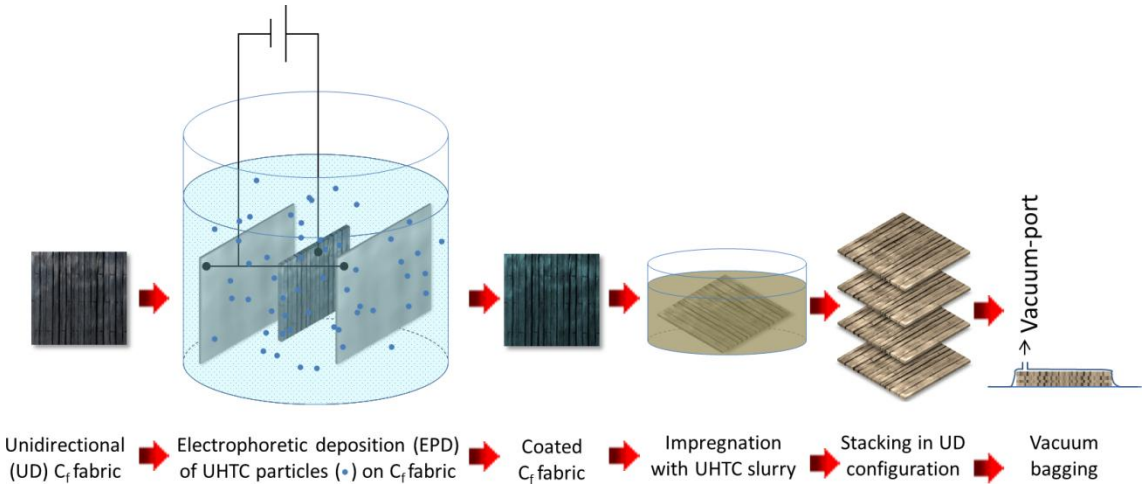

Fig.1. Schematic flow diagram of green shaping.

Table 1 Sample ID and nominal matrix and coating composition

Table 1. Composition of UHTCMC materials

Sample ID	**Matrix**	**coating**
ZZ	ZrB_2 + 5vol% B_4C	ZrB_2
ZT	ZrB_2 + 5vol% B_4C	TiB_2
TZ	TiB_2 + 5vol% B_4C	ZrB_2
Z	ZrB_2 + 5vol% B_4C	Uncoated

2.3. Microstructure and mechanical characterization

The bulk densities after sintering were measured by Archimedes' method. FVC was calculated by multiplying fiber mass per unit area, times the layers' number and sample area. The microstructures were analyzed with Field-Emission Scanning Electron Microscopy (FESEM, mod. ΣigmaCarl Zeiss NTS Gmbh Öberkochen, Germany) coupled with Energy Dispersive X-ray Spectroscopy (EDXS, mod. INCA energy 300; Oxford instruments, High Wycombe, UK). Cross section of coated carbon bundle was prepared by cutting a single bundle with a razor blade. Cross sections of sintered samples were polished down to 0.25 µm finish with diamond abrasive by using semi-automatic polishing machine (Tegramin-25, Stuers, Italy). The residual porosity of the sintered materials was measured by using the Image-Pro Analyzer 7.0 software (v.7, Media Cybernetics, USA) to calculate the fraction of the area covered by pores on the FESEM images of polished sections. The measurement was based on the assumption that pores have a shape factor of one. In this way the ratio of the number of pixels attributed to the pores to the total number of pixels in the image (1024×768 pixels resolution) corresponds to the volumetric fraction. 4-point flexural strength (σ) and fracture toughness (K_{Ic}) were measured on 25×2.5×2 mm^3 (length × width × thickness) bars, and (25×2×2.5 mm^3, length x width x thickness) chevron notched beams (CNBs), respectively. CNBs were notched with a 0.1 mm thick diamond saw. Both tests were performed at room temperature by using a fully articulated steel 4-point fixture with a lower span of 20 mm and an upper span of 10 mm on Zwick-Roell Z050 testing machine. The crosshead speed was 1 mm/min and 0.05 mm/min to measure σ and K_{Ic}, respectively. The WoF was calculated from the test of CNB as the area below the load-

displacement curve divided by the double of the projected real surface. The total WoF was broken down as the area pre- and post-peak, W_T and W_W respectively.

3. Result and discussion

3.1. EPD microstructure

Fig.2 and 3 show C_f bundles coated with ZrB_2 or TiB_2, respectively, by applying electric fields and deposition time between 6 and 11 V/cm, and 5 and 10 min, respectively. It can be seen that the deposited coating increases gradually with the applied electric field and deposition time for both the suspensions. The thickest and most compact coatings were obtained by applying the electric field of 11 V/cm.

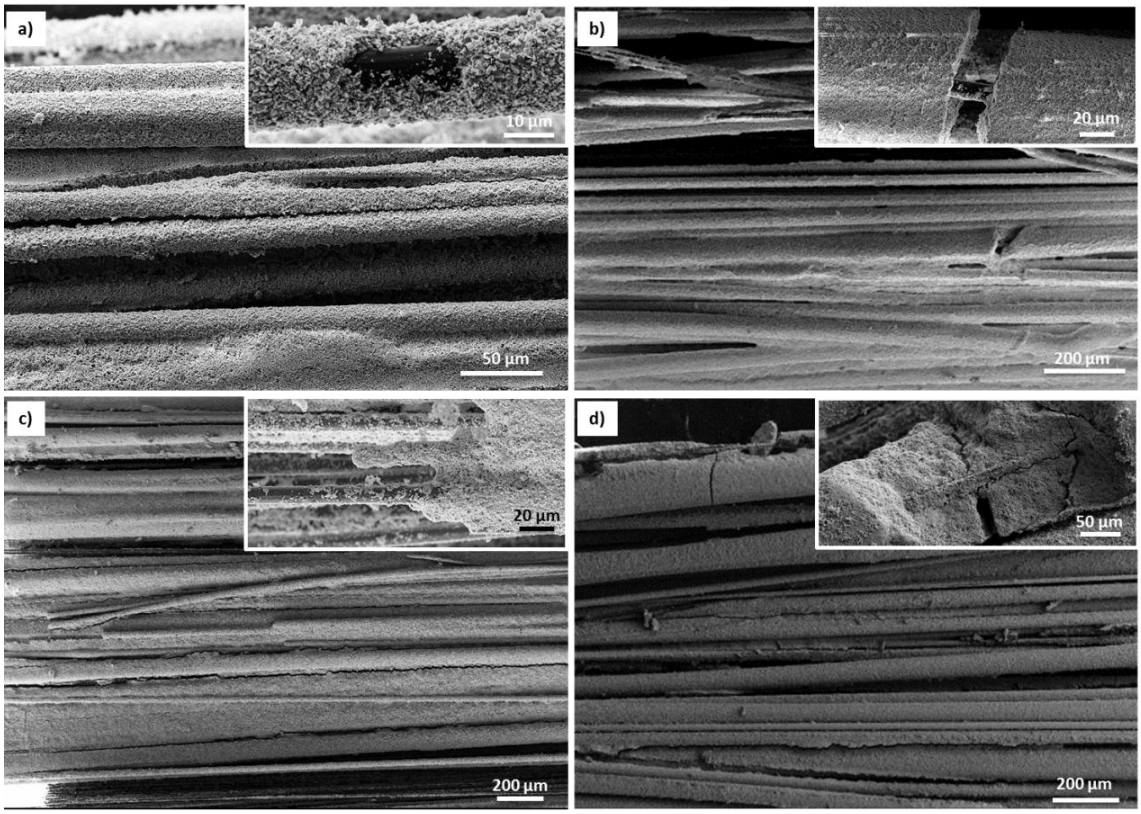

Fig.2. Carbon fibers covered with ZrB_2 by EPD at different applied electric field and time: (a) 6 V/cm, 5 min, (b) 11 V/cm, 5 min, (c) 6 V/cm, 10 min, (d) 11 V/cm, 10 min.

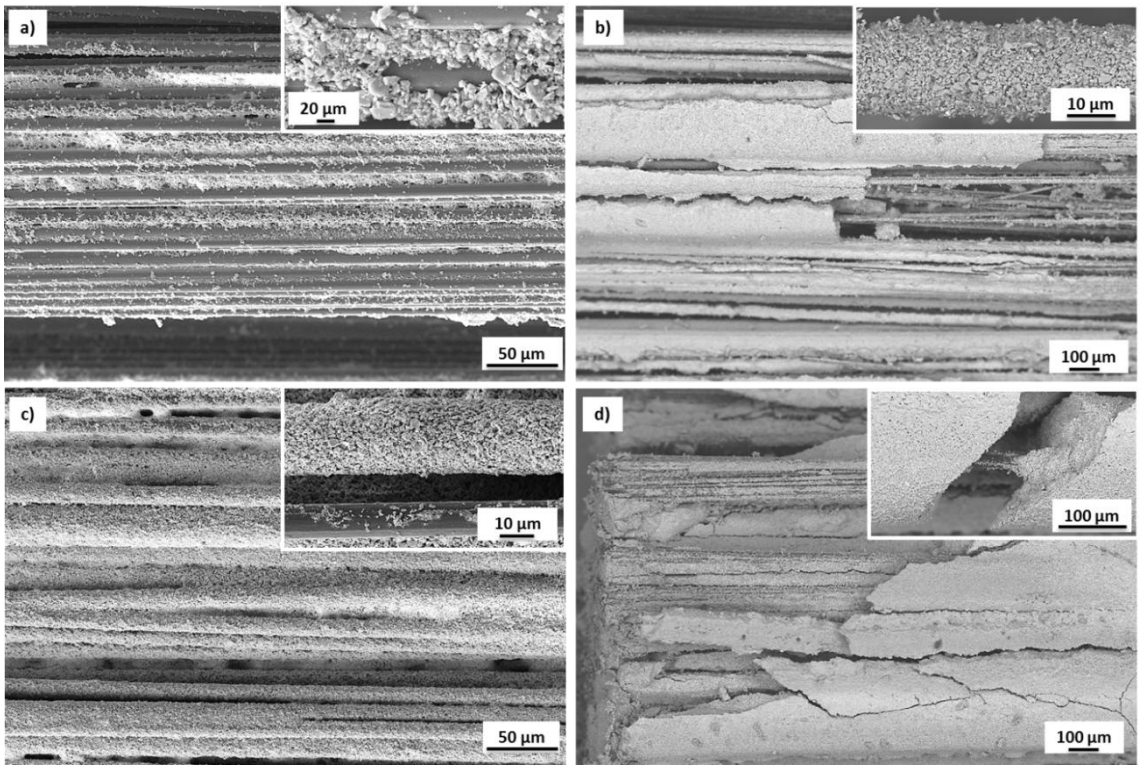

Fig.3. Carbon fibers covered with TiB_2 by EPD at different applied electric field and time; (a) 6 V/cm, 5 min, (b) 11 V/cm, 5 min, (c) 6 V/cm, 10 min, (d) 11 V/cm, 10 min.

In order to ensure a compact coating and minimize crack formation, 11 V/cm and 100 s were selected as electric field and deposition time, respectively. Fig.4 shows the cross section of C_f bundle after EPD of ZrB_2 obtained under the latter process parameters. EPD produced an external ZrB_2 layer of 15-20 µm thick where the particles are well packed to each other and well stuck to the C_f surface. The cracks on the film and the fibers spreading should be ascribed to the sample preparation. The coating was formed by particles smaller than 4 µm (the larger particles sediment) and penetrated inside the bundle up to about 100 µm. After that, the inner fibers present a discontinuous coating, being coated by few ZrB_2 particles.

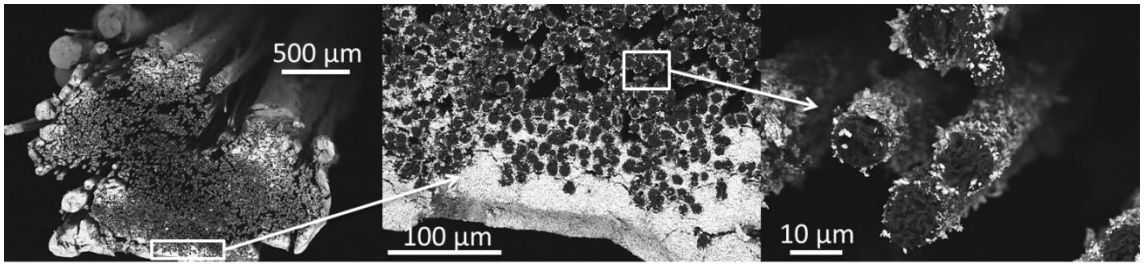

Fig.4. Cross section of a single bundle of C_f covered with ZrB_2 by applying an electric field of 11 V/cm for 100 s.

3.2. Sintered UHTCMC microstructures

- ZZ (ZrB_2-based matrix and ZrB_2 coating) is characterized by a fully dense microstructure with a relative density of 4.1 g/cm^3 and a residual porosity of just 2.1 vol%. The material has 40 vol% of fiber and shows a non-periodic structure (so called "salami" structure [23]) due to the discrete distribution of the bundles inside the matrix, favored by EPD (Fig.5 (a)). Bundles are 200-600 µm thick and about 2 mm wide, as in the original fabrics. EPD covers only the outer shell of each strand (less than 5 layers of C_f [23]), resulting in a well stuck external thick layer of 15–20 µm, while the slurry mostly fills the spaces between the covered bundles, which preserves their pristine configuration also after sintering. Dark spots within the ZrB_2 matrix (the gray area in Fig.5 (b)) are B_4C grains, characterized by a lower density, 2.5 g/cm^3, compared to the ZrB_2 (6.1 g/cm^3). Observing Fig.5 (b), it is possible to recognize a B_4C-free area at the fiber/matrix interface, 15 µm thick, that can be ascribed to the EPD ZrB_2 coating. The fiber/coating interfaces are characterized by jagged profiles.

-ZT (ZrB_2-based matrix and TiB_2 coating) is well densified and presents characteristics in common with both the first two samples (Fig.5 (d)): relative density of 3.8 g/cm^3, 37 vol% of fiber, jagged TiB_2-coating/matrix interface (due to the sintering stresses [23]),

and discrete distribution (non-periodic) of fiber bundles in the matrix. On the other hand, ZT presents a thicker coating, approximately 30-50 µm.

- TZ (TiB_2-based matrix and ZrB_2 coating) shows 3.9 g/cm^3 of density and 33 vol% of fiber. ZrB_2 coating of about 7-20 µm is well recognizable from the matrix due to different contrast displayed in SE/BSE imaging (Fig.5 (c)). Also in this case the ZrB_2-coated carbon fiber bundles keep memory of the structure of the pristine bundles of the fabrics, displaying a "salami" or non-periodic structure.

-Z (ZrB_2-based matrix, no coating): a polished section of this sample, Fig.5 (e and f) reveals the completely different texture of this sample, displaying a homogeneous distribution of C_f inside the matrix. This homogeneous C_f distribution can be described as a periodic configuration, to distinguish it from the non-periodic one of EPD treated samples. Single bundles in periodic case are hardly recognizable. Dark pockets are B_4C particles. The density is 3.97 g/cm^3, the amount of fiber is 39 vol%. Residual porosity by image analysis is 7.3 %.

Table 2: Microstructural and mechanical properties. ρ: density; p: porosity; FVC: fiber volume content; K_{Ic}: fracture toughness; W_T: work of fracture at the crack tip; W_W: work of fracture on the crack wake.

Sample	ρ (g/cm^3)	p (%)	FVC (vol%)	σ (MPa)	K_{Ic} (MPa√m)	W_T (J/m^2)	W_W (J/m^2)
ZZ	4.1	2.1	40	284±39	11.0±2.4	413±158	954±233
ZT	3.8	8.8	37	278±26	10.7±2.0	333±50	850±391
TZ	3.9	9.2	33	169±23	10.8±0.5	281±56	668±190
Z	4	7.3	39	326±16	7.9±0.7	392±22	500±130

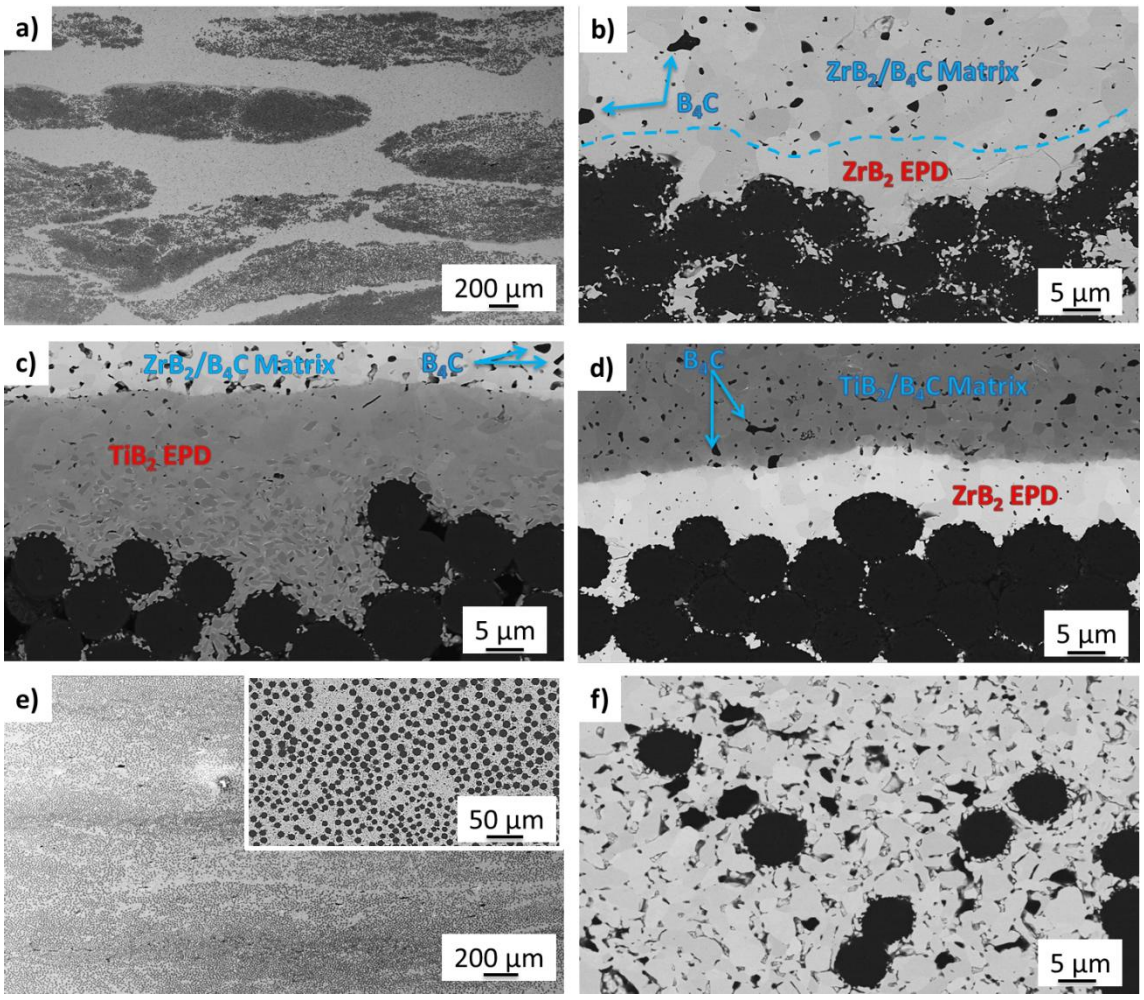

Fig.5. SEM micrograph of polished cross section of (a,b) ZZ sample, (c) ZT sample, (d) TZ sample, and (e,f) Z sample.

3.3. Mechanical properties

Values of strength and fracture toughness for the produced samples are reported in Table 2. The uncoated material, Z, has the highest strength (~330 MPa) due to homogeneous microstructure, which ensures the good mechanical stresses transfer between matrix and fibers. ZZ and ZT, with ZrB_2 matrix and ZrB_2 or TiB_2 coating

respectively, both display a σ of ~280 MPa, independent of the different nature of the coating and the different fraction of residual porosity. Sample TZ, with TiB_2 matrix and ZrB_2 coating has the lowest strength, ~170 MPa, probably due to the lowest FVC (Fig.6 (a)). In Fig.6 (a,b), experimental data of σ, K_{Ic}, W_T, and W_W for non-periodic and periodic microstructures are plotted as function of FVC in order to assess whether or not there is some dependence. In case of σ a linear dependence on FVC is expected. In fact, due to the iso-strain condition imposed by the test configuration σ is a linear function of FVC according with the linear rule of mixtures:

$$\sigma = \sigma_f \cdot V_f + \sigma_m(1 - V_f) \quad (1)$$

where V_f is FVC, σ_f and σ_m are the strength of the fiber (3.4 GPa) and the matrix (65 MPa [9]), respectively. The lack of fit of the linear regression between σ and FVC (R^2 = 0.88) and the gap of about 80% between the experimental values and the predicted ones by Eq.(1) can be mainly addressed to mixed failure mode (tensile + shear), which underestimates the apparent measured σ, and to the concomitance of others microstructural variables such as porosity, matrix and coating composition, fibers alignment, etc. Anyway, it is reasonable to say that σ depends more on FVC rather than fiber distribution degree. In fact, the correlation coefficient (r) indicates a strong agreement between σ and FVC both in the case we consider all the samples (r = +0.91) and in the case we exclude Z (r = +0.92). It is worth to remind that r = +1 indicates the strongest possible agreement, and r = −1 the strongest possible disagreement.

As for the toughness, the striking difference the periodic Z baseline material, 7.7 MPa√m, and the non-periodic (EPD derived) samples, about 11 MPa√m, confirms the EPD-step effect on the mechanical properties. This large increment of toughness was attributed to the specific texture obtained, where the discrete distribution of carbon

bundles inside the matrix (non-periodic distribution) allows the synergic activation of diverse toughening mechanisms that contributed to enhance the overall toughness and damage tolerance [23]. In particular the bundles, owing to the presence of weak C_f/C_f or C_f/ZrB_2 interfaces inside (as sketched in Fig.6 (c)), allows a large pull-out length according with the adapted the Kelly-Tyson model [23]:

$$l_c = \frac{\sigma \cdot r}{\tau} \quad (2)$$

where l_c is the pull-out length, σ and r are the critical stress and the equivalent radius of the bundle, respectively, and τ is the critical shear stress of the weaker C_f/C_f or C_f/ZrB_2 interfaces. In fact, contrary to the σ trend, K_{Ic} is strongly affected by the degree of fiber dispersion as proved by the increase of r from -0.32 to +0.68 with the Z value exclusion. In Fig.6 (a), it can be seen how the fracture toughness increases with the increasing of FVC and is boosted by the so called "salami" structure [23] realized in the non-periodic sample. The toughness value of periodic Z sample appears as an outlier point 27% lower than the linear regression fitting of the non-periodic samples. The low r value of +0.68 reflects the dubious validity, in case of continuous-fiber-reinforced ceramic matrix composites, of the K_{Ic} values. Even if it is praxis to provide toughness values for CMCs, not always the crack-stability criterion is investigated, and the tests with CNBs could not simultaneously fulfill the plane-strain condition and limited crack tip plasticity (microcracking, fiber debonding, etc.). Moreover in the case of CMCs, the current standards do not establish any specimen-size criteria to take into account the crack wake plasticity (fiber/boundless pull-out). These phenomena, typical belonging to the continuous-fiber-reinforced composites, are in contrast with the usual assumption of a flat crack-growth-resistance curve, and could lead to extend the stable crack growth beyond the maximum load. For the above reasons, giving a valid K_{Ic} determination

method for UHTCMCs is challenging. To avoid this tricky point, we performed a WoF analysis. The idea (sketched in Fig.6 (d)) is to correlate the work spent to reach the maximum load (W_T), and the following work spent up to the ultimate displacement (W_W) to the toughening mechanisms activated ahead of the crack tip (microcracking, fiber debonding, etc.), and on crack wake (fiber/bundle pull-out), respectively. This analysis suggests that the toughening mechanisms ahead of the crack tip are enhanced by FVC, and are independent of fiber distribution degree (Fig.6 (b)). In fact, r remains roughly the same (+0.98) whether we consider the periodic structure or not. On the contrary, W_W is strongly affected by the degree of fiber dispersion (Fig.6 (c)) as proved by the increase of r from +0.24 to +0.997 with the Z value exclusion. The obtained value of r = +0.997, is in agreement with the expected behaviour of the toughening contributions, and reinforces the hypothesis behind the used WoF analysis. On the other hand, no strong correlations were identified between the investigated mechanical properties and the microstructural features, such as matrix and coating composition, coating thickness, and porosity. The mechanical properties of the investigated materials seem to be controlled by FVC and its distribution degree (periodic or non-periodic structure).

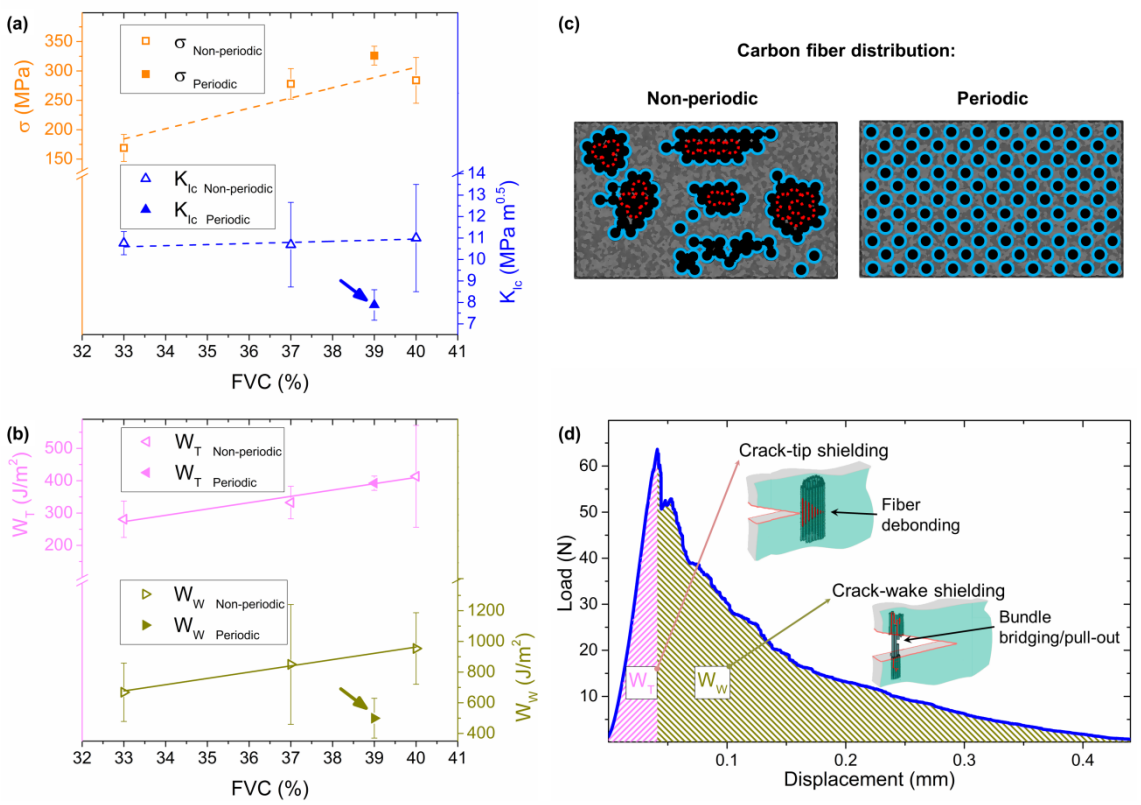

Fig.6. (a) Flexural strength, σ, and fracture toughness, K_{Ic}, as function of the fiber volume content (FVC). (b) Work of fracture at the crack tip, W_T, and work of fracture at the crack wake, W_W, vs. FVC. Left hand ordinates refer to the distribution-independent properties: σ and W_T. Right hand ordinates refer to the distribution-dependent properties: K_{Ic} and W_W. Arrows point the outlier points. (c) Sketch of non-periodic (salami-inspired architecture) and periodic carbon fiber distribution, where strong and weak interfaces are highlighted with solid blue lines and sotted red lines, respectively. (d) Load vs. displacement curve obtained whit the chevron-notched three-point bend fracture toughness technique. (For interpretation of the references to colour in this figure legend, the reader is referred to the web version of this article.)

A possible implication of the proposed WoF analysis is that to use it as test to evaluate pull-out toughening, which is proportional to W_W. The WoF analysis is easier to perform respect to push-in and push-out techniques which requires thin sample. In fact, the thickness should be less than one-tenth compared to the diameter of the fiber in order to avoid fiber buckling. Moreover, if high thermal residual stresses are present, as for the case of UHTCMCs, the machining can induce a stress releasing as a consequence of the matrix cracking [34].

4. Conclusions

The deposition of UHTC coating on carbon fabrics through EPD process is shown. The slurry infiltration of coated carbon fabric fills the intra-fiber woven regions without affects the outer EPD coating which successfully withstands subsequent manufacturing steps of UHTCMCs. The EPD derived samples show a non-periodic carbon fiber distribution.

Evaluation of the fiber volume content (FVC) on the UHTCMCs fracture resistance, including fracture strength (σ), fracture toughness (K_{Ic}), work of fracture (WoF) at the crack tip (W_T), and WoF at the crack wake (W_W), indicates that:

- higher FVC, in the range of 33-40 %, generates higher σ, K_{Ic}, W_T, and W_W.
- K_{Ic} and W_W are highly sensitive to the degree of fiber distribution, whereas σ and W_T are not.
- Non-periodic specimens, characterized by “salami” substructures, exhibit higher fracture resistance than periodic samples. Hence, the crack shielding can be enhanced by a non-periodic distribution of the fibers.

Acknowledgements

Part of this work was funded by Ministero degli Affari Esteri e della Cooperazione Internazionale (MAECI - Italy) in the framework of Progetto di Grande Rilevanza: "ULTRAHIGH TEMPERATURE CERAMIC MATRIXCOMPOSITES BY ADDITIVE MANUFACTURING USING POLYMER PRECURSORS". This work also received support by the European Union's Horizon 2020 research and innovation programme under Grant Agreement no 685594. (C3HARME: Next Generation Ceramic Composites for Harsh Combustion Environment and Space). C. Melandri and D. dalle Fabbriche are gratefully acknowledged for technical support.

References

[1] W.G. Fahrenholtz, G.E. Hilmas, I.G. Talmy, J.A. Zaykoski, Refractory diborides of zirconium and hafnium, J. Am. Ceram. Soc. 90 (2007) 1347–1364. doi:10.1111/j.1551-2916.2007.01583.x.

[2] E. Wuchina, E. Opila, M. Opeka, W. Fahrenholtz, I. Talmy, UHTCs: Ultra-high temperature ceramic materials for extreme environment applications, Soc. Interface. (2007) 30–36.

[3] F. Monteverde, A. Bellosi, L. Scatteia, Processing and properties of ultra-high temperature ceramics for space applications, Mater. Sci. Eng. A. 485 (2008) 415–421. doi:10.1016/j.msea.2007.08.054

[4] G. Zhang, W. Guo, D. Ni, Y. Kan, Ultrahigh temperature ceramics (UHTCs) based on ZrB_2 and HfB_2 systems: powder synthesis, densification and mechanical properties, J. Phys. Conf. Ser. 176 (2009) 1–12. doi:10.1088/1742-6596/176/1/012041

[5] A.L. Chamberlain, W.G. Fahrenholtz, G.E. Hilmas, D.T. Ellerby, Characterization

of zirconium diboride for thermal protection systems, Euro Ceram. Viii, Pts 1-3. 264–268 (2004) 493–496. doi:10.4028/www.scientific.net/KEM.264-268.493

[6] R. Savino, M. De Stefano Fumo, D. Paterna, M. Serpico, Aerothermodynamic study of UHTC-based thermal protection systems, Aerosp. Sci. Technol. 9 (2005) 151–160. doi:10.1016/j.ast.2004.12.003

[7] W. Krenkel, Ceramic matrix composites: fibre reinforced ceramics and their applications, WILEY-VCH Verlag GmbH & Co. KGaA, Weinheim, 2008. doi:10.1002/9783527622412

[8] F. Breede, R. Jemmali, H. Voggenreiter, D. Koch, Design and testing of a C/C-SiC nozzle extension manufactured via filament winding technique and liquid silicon infiltration, in: D. Singh, D. Zhu, W.M. Kriven, S. Mathur (Eds.) Design, development, and applications of structural ceramics, composites, and nanomaterials John Wiley & Sons, Inc., Hoboken, 2014, pp. 3–14. doi:10.1002/9781118889770.ch1

[9] L. Zoli, A. Vinci, P. Galizia, C. Melandri, D. Sciti, On the thermal shock resistance and mechanical properties of novel unidirectional UHTCMCs for extreme environments, Sci. Rep. 8 (2018) 9148. doi:10.1038/s41598-018-27328-x

[10] D. Sciti, L. Zoli, L. Silvestroni, A. Cecere, G.D. Di Martino, R. Savino, Design, fabrication and high velocity oxy-fuel torch tests of a C_f-ZrB_2- fiber nozzle to evaluate its potential in rocket motors, Mater. Des. 109 (2016) 709–717. doi:10.1016/j.matdes.2016.07.090

[11] L. Zoli, D. Sciti, Efficacy of a ZrB_2–SiC matrix in protecting C fibres from oxidation in novel UHTCMC materials, Mater. Des. 113 (2017) 207–213. doi:10.1016/j.matdes.2016.09.104

[12] S. Tang, J. Deng, S. Wang, W. Liu, K. Yang, Ablation behaviors of ultra-high

temperature ceramic composites, Mater. Sci. Eng. A. 465 (2007) 1–7. doi:10.1016/j.msea.2007.02.040

[13] A.R. Boccaccini, I. Zhitomirsky, Application of electrophoretic and electrolytic deposition techniques in ceramics processing, Curr. Opin. Solid State Mater. Sci. 6 (2002) 251–260. doi:10.1016/S1359-0286(02)00080-3

[14] L. Besra, M. Liu, A review on fundamentals and applications of electrophoretic deposition (EPD), Prog. Mater. Sci. 52 (2007) 1–61. doi:10.1016/j.pmatsci.2006.07.001

[15] P. Sarkar, P.S. Nicholson, Electrophoretic deposition (EPD): mechanisms, kinetics and application to ceramics, J. Am. Ceram. Soc. 79 (1996) 1987–2002. doi:10.1111/j.1151-2916.1996.tb08929.x

[16] I. Zhitomirsky, L. Gal-Or, Formation of hollow fibers by electrophoretic deposition, Mater. Lett. 38 (1999) 10–17. doi:10.1016/S0167-577X(98)00124-4

[17] R.V. Subramanian, E.A. Nyberg, Zirconia and organotitanate film formation on graphite fiber reinforcement for metal matrix composites, J. Mater. Res. 7 (1992) 677–688. doi:10.1557/JMR.1992.0677

[18] J.-H. Lee, G.-Y. Gil, D.-H. Yoon, Fabrication of SiC_f /SiC composites using an electrophoretic deposition, J. Korean Ceram. Soc. 46 (2009) 447–451. doi:10.4191/KCERS.2009.46.5.447

[19] I. Zhitomirsky, Electrophoretic and electrolytic deposition of ceramic coatings on carbon fibers, J. Eur. Ceram. Soc. 18 (1998) 849–856. doi:10.1016/S0955-2219(97)00213-6

[20] J.B. Davis, J.P.A. Lofvander, A.G. Evans, E. Bischoff, M.L. Emiliani, Fiber coating concepts for brittle-matrix composites J. Am. Ceram. Soc. 76 (1993) 1249–1257. doi:10.1111/j.1151-2916.1993.tb03749.x

[21] K. Yoshida, Y. Aoyagi, H. Akimoto, T. Yano, M. Kotani, T. Ogasawara, Interfacial control of uni-directional SiC_f/SiC composites based on electrophoretic deposition and their mechanical properties, Compos. Sci. Technol. 72 (2012) 1665–1670. doi:10.1016/j.compscitech.2012.07.004

[22] K.E. Gonsalves, R. Yazici, S. Han, Ceramic coatings for graphite fabrics by metalorganic pyrolysis, J. Mater. Sci. Lett. 10 (1991) 834–837. doi:10.1007/BF00724753

[23] P. Galizia, S. Failla, L. Zoli, D. Sciti, Tough salami-inspired C_f/ZrB_2 UHTCMCs produced by electrophoretic deposition, J. Eur. Ceram. Soc. 38 (2018) 403-409. doi:10.1016/j.jeurceramsoc.2017.09.047

[24] X. Zhang, Y. Hou, P. Hu, W. Han, J. Luo, Dispersion and co-dispersion of ZrB_2 and SiC nanopowders in ethanol, Ceram. Int. 38 (2012) 2733–2741. doi:10.1016/j.ceramint.2011.11.042

[25] S.H. Lee, Y. Sakka, Y. Kagawa, Dispersion behavior of ZrB_2 powder in aqueous solution, J. Am. Ceram. Soc. 90 (2007) 3455–3459. doi:10.1111/j.1551-2916.2007.01949.x

[26] Y. Zhang, X. Lin, Aqueous electrophoretic deposition of ZrB_2-SiC nano-composites in pulsed DC electric fields, Adv. Automob. Eng. 01 (2016) 1–3. doi:10.4172/2167-7670.S1-003

[27] F. Tang, T. Uchikoshi, K. Ozawa, Y. Sakka, Dispersion of SiC suspensions with cationic dispersant of polyethylenimine, J. Ceram. Soc. Japan. 113 (2005) 584–587. doi:10.2109/jcersj.113.584

[28] J. Tabellion, R. Clasen, Electrophoretic deposition from aqueous suspensions for near-shape manufacturing of advanced ceramics and glasses, J. Mater. Sci. 39 (2004)

803–811. doi:10.1023/B:JMSC.0000012907.52051.fb

[29] H. Negishi, Uniform and ultra low-power electrophoretic deposition of silica powder using a nonflammable organic solvent, J. Eur. Ceram. Soc. 36 (2016) 285–290. doi:10.1016/j.jeurceramsoc.2015.07.032

[30] C. Mendoza, Z. González, Y. Castro, E. Gordo, B. Ferrari, Improvement of TiN nanoparticles EPD inducing steric stabilization in non-aqueous suspensions, J. Eur. Ceram. Soc. 36 (2016) 307–317. doi:10.1016/J.JEURCERAMSOC.2015.06.023.

[31] P. Galizia, I.V. Ciuchi, D. Gardini, C. Baldisserri, C. Galassi, Bilayer thick structures based on $CoFe_2O_4/TiO_2$ composite and niobium-doped PZT obtained by electrophoretic deposition, J. Eur. Ceram. Soc. 36 (2016). doi:10.1016/j.jeurceramsoc.2015.07.038

[32] R. Zehbe, C. Mochales, D. Radzik, W.-D. Müller, C. Fleck, Electrophoretic deposition of multilayered (cubic and tetragonal stabilized) zirconia ceramics for adapted crack deflection, J. Eur. Ceram. Soc. 36 (2016) 357–364. doi:10.1016/j.jeurceramsoc.2015.08.022

[33] D. Sciti, L. Silvestroni, V. Medri, F. Monteverde, Sintering and densification of ultra-high temperature ceramics, in: W.G. Fahrenholtz, E.J. Wuchina, W.E. Lee, Y. Zhou (Eds.), Ultra-High Temp. Ceram. Mater. Extrem. Environ. Appl., Wiley & Sons, Inc., John, 2014, pp.112–143.

[34] P. Galizia, L. Zoli, D. Sciti, Impact of residual stress on thermal damage accumulation, and Young's modulus of fiber-reinforced ultra-high temperature ceramics, Mater. Des. 160 (2018) 803–809. doi:10.1016/j.matdes.2018.10.019